Calhoun
Institutional Archive of the Naval Postgraduate School

Calhoun: The NPS Institutional Archive

DSpace Repository

Theses and Dissertations | 1. Thesis and Dissertation Collection, all items

2011-12

Characterization of the MEMS directional sound sensor in the high frequency (15 - 20 kHz) range

Davis, Darren D.

Monterey, California. Naval Postgraduate School

https://hdl.handle.net/10945/10588

This publication is a work of the U.S. Government as defined in Title 17, United States Code, Section 101. Copyright protection is not available for this work in the United States.

Downloaded from NPS Archive: Calhoun

http://www.nps.edu/library

Calhoun is the Naval Postgraduate School's public access digital repository for research materials and institutional publications created by the NPS community. Calhoun is named for Professor of Mathematics Guy K. Calhoun, NPS's first appointed -- and published -- scholarly author.

Dudley Knox Library / Naval Postgraduate School
411 Dyer Road / 1 University Circle
Monterey, California USA 93943

NAVAL POSTGRADUATE SCHOOL

MONTEREY, CALIFORNIA

THESIS

CHARACTERIZATION OF THE MEMS DIRECTIONAL SOUND SENSOR IN THE HIGH FREQUENCY (15–20 kHz) RANGE

by

Darren D. Davis

December 2011

Thesis Co-Advisors: Gamani Karunasiri
Bruce Denardo

Approved for public release; distribution is unlimited

THIS PAGE INTENTIONALLY LEFT BLANK

REPORT DOCUMENTATION PAGE			Form Approved OMB No. 0704–0188
Public reporting burden for this collection of information is estimated to average 1 hour per response, including the time for reviewing instruction, searching existing data sources, gathering and maintaining the data needed, and completing and reviewing the collection of information. Send comments regarding this burden estimate or any other aspect of this collection of information, including suggestions for reducing this burden, to Washington headquarters Services, Directorate for Information Operations and Reports, 1215 Jefferson Davis Highway, Suite 1204, Arlington, VA 22202–4302, and to the Office of Management and Budget, Paperwork Reduction Project (0704–0188) Washington DC 20503.			
1. AGENCY USE ONLY *(Leave blank)*	**2. REPORT DATE** December 2011	**3. REPORT TYPE AND DATES COVERED** Master's Thesis	
4. TITLE AND SUBTITLE Characterization of the MEMS Directional Sound Sensor in the High Frequency (15–20 kHz) Range		**5. FUNDING NUMBERS**	
6. AUTHOR(S) Darren D. Davis			
7. PERFORMING ORGANIZATION NAME(S) AND ADDRESS(ES) Naval Postgraduate School Monterey, CA 93943–5000		**8. PERFORMING ORGANIZATION REPORT NUMBER**	
9. SPONSORING /MONITORING AGENCY NAME(S) AND ADDRESS(ES) N/A		**10. SPONSORING/MONITORING AGENCY REPORT NUMBER**	
11. SUPPLEMENTARY NOTES The views expressed in this thesis are those of the author and do not reflect the official policy or position of the Department of Defense or the U.S. Government. IRB Protocol number ____N/A_____.			
12a. DISTRIBUTION / AVAILABILITY STATEMENT Approved for public release; distribution is unlimited		**12b. DISTRIBUTION CODE** A	

13. ABSTRACT (maximum 200 words)

The Sensor Research Laboratory (SRL) at Naval Postgraduate School (NPS) has developed a micro-electromechanical system (MEMS) based directional sound sensors that mimics the aural system of the Ormia Ochracea Fly. The goal of this research is to characterize a set of directional sound sensors with varying configurations that operate in the high frequency range (15–20 kHz). The sensor consists of two identical wings coupled in the middle and the entire structure is connected to a substrate using two legs in the middle. In response to sound, the coupled wings oscillate with rocking and bending like motions at frequencies that depend on the mechanical characteristics of the structure. A simulation of sensor characteristics using COMSOL finite element software showed a resonant frequency of about 20 kHz for each device. The devices were fabricated by the MEMSCAP foundry service using silicon-on-insulator (SOI) substrate with a 25 μm device layer. Using a laser vibrometer, response to incident sound pressure was measured at different frequencies and angles. All the devices showed that measured and simulated frequencies were in reasonably close agreement. The measurements showed good sensitivity to the direction of sound as predicted.

14. SUBJECT TERMS MEMS, Ormia, Ormia Ochracea, Directional Microphone, Sensor, Fly Hearing, High Frequency			**15. NUMBER OF PAGES** 51
			16. PRICE CODE
17. SECURITY CLASSIFICATION OF REPORT Unclassified	**18. SECURITY CLASSIFICATION OF THIS PAGE** Unclassified	**19. SECURITY CLASSIFICATION OF ABSTRACT** Unclassified	**20. LIMITATION OF ABSTRACT** UU

NSN 7540–01–280–5500

Standard Form 298 (Rev. 8–98)
Prescribed by ANSI Std. Z39.18

THIS PAGE INTENTIONALLY LEFT BLANK

Approved for public release; distribution unlimited

CHARACTERIZATION OF THE MEMS DIRECTIONAL SOUND SENSOR IN THE HIGH FREQUENCY (15 – 20 kHz) RANGE

Darren D. Davis
Lieutenant, United States Navy
B.S., Old Dominion University, 2005

Submitted in partial fulfillment of the
requirements for the degree of

MASTER OF SCIENCE IN APPLIED PHYSICS

from the

NAVAL POSTGRADUATE SCHOOL

December 2011

Author: Darren D. Davis

Approved by: Gamani Karunasiri
Thesis Co-Advisor

Bruce Denardo
Thesis Co-Advisor

Andres Larraza
Chair, Department of Physics

THIS PAGE INTENTIONALLY LEFT BLANK

ABSTRACT

The Sensor Research Laboratory (SRL) at Naval Postgraduate School (NPS) has developed a micro-electromechanical system (MEMS) based directional sound sensors that mimics the aural system of the Ormia Ochracea Fly. The goal of this research is to characterize a set of directional sound sensors with varying configurations that operate in the high frequency range (15–20 kHz). The sensor consists of two identical wings coupled in the middle and the entire structure is connected to a substrate using two legs in the middle. In response to sound, the coupled wings oscillate with rocking and bending like motions at frequencies that depend on the mechanical characteristics of the structure. A simulation of sensor characteristics using COMSOL finite element software showed a resonant frequency of about 20 kHz for each device. The devices were fabricated by the MEMSCAP foundry service using silicon-on-insulator (SOI) substrate with a 25 μm device layer. Using a laser vibrometer, response to incident sound pressure was measured at different frequencies and angles. All the devices showed that measured and simulated frequencies were in reasonably close agreement. The measurements showed good sensitivity to the direction of sound as predicted.

THIS PAGE INTENTIONALLY LEFT BLANK

TABLE OF CONTENTS

THIS PAGE INTENTIONALLY LEFT BLANK

LIST OF FIGURES

THIS PAGE INTENTIONALLY LEFT BLANK

LIST OF TABLES

THIS PAGE INTENTIONALLY LEFT BLANK

ACKNOWLEDGMENTS

Thank you, Professor Gamani Karunasiri for your continuous support and guidance throughout the completion of this thesis. Your patience throughout this period of research has been noteworthy. Dr. Karunasiri's mentorship allowed me not only to understand the physics of the research, but also how to conduct my own research.

Thank you, Professor Bruce Denardo for your help and guidance in this thesis process. Dr. Denardo's questioning attitude and his resolve to ensure things are what they seem are inspiring.

In addition, thank you to Sam Barone for your help in getting our power supply fixed so that we were able to continue using the Vibsoft® computer program for the laser vibrometer. Sam also took great photos of the devices with his microscope. George Jaksha, our machinist, has drilled countless holes and made several device mounts that were instrumental in helping us realize we were getting sound diffraction that was causing a zero net pressure. He often accomplished these tasks on short notice and very quickly as well. Jay Adeff took several of the photos used in this thesis as well. Thank you for your willingness and patience in getting the right photo.

Finally, thank you to my wife, Kelly, and my children, Chaela and Gavin, for their unconditional support, patience, and understanding during my time at the Naval Postgraduate School.

THIS PAGE INTENTIONALLY LEFT BLANK

I. INTRODUCTION

A. MOTIVATION

Necessity is the mother of all invention. Charles Darwin could have considered this when postulating his theory of natural selection, which is an important process by which evolution takes place among a population of species. Survival is necessary and nature has invented and solved many problems that humans face on a daily basis. Throughout the millennia, natural selection provides a filter for determining which animals survive and which do not. If the animal's life depends on its hearing abilities, due to either mate selection or finding a source of food, then those animals with better hearing will prevail [1].

This thesis examines performances of a directional sound sensor that mimics the Ormia ochracea fly. When an animal processes sensory information, especially as a prelude to orientation or locomotion, few tasks are more important than determining the incident direction of a stimulus [2]. For humans, sound energy travels through the medium from the source to our ear. The ear funnels the sound energy onto our eardrum. The energy is passed from an air domain to a fluid domain and is then transmitted to our central nervous system. We can determine the approximate angle of arrival of the sound energy because we have two distinct ears. The sound energy will typically hit one ear first and then the other ear. Our brain calculates this angle subconsciously and we know from which angle the sound originated [1].

A small fly, *Ormia Ochracea*, has developed a unique sense of hearing, and a remarkable ability to localize sound sources, which allows it to continue to survive [2]. This fly has a very small auditory system that allows quick and easy determination of incident sound angle. By mimicking this fly's hearing, we can produce a sound sensor with similar directional abilities [1].

B. BACKGROUND

The basis of this thesis is the directional sensor designed at the Sensor Research Laboratory (SRL) of the Naval Postgraduate School at Monterey, California. The SRL at NPS has designed and developed several generations of MEMS-based devices. This project has resulted in the completion of several theses at NPS. This thesis expands on previous work done and introduces a new frequency range for the MEMS-based devices. The main goal of this thesis is to characterize six devices designed to operate in the high frequency range (15–20 kHz). This will allow further modeling and simulation to gain a thorough understanding of the directional sensor in the high frequency range.

C. ORMIA OCHRACEA

Ormia Ochracea is a parasitic fly common to the southern United States and Mexico. Given the small size of this fly, it has a remarkable ability to determine the direction of sound. This ability is crucial to the fly's survival [3]. In order to reproduce, the female fly must find and deposit her parasitic larvae on a live field cricket. The female fly locates her host at night, relying on auditory cues from the cricket's mating call [2].

The *Ormia ochracea* has the ability to locate a cricket acoustically despite the fact that its sensors are only separated by approximately 1.5 mm, versus a source wavelength of approximately 7 cm [4]. This difference leads to extremely small interaural intensity and time of arrival differences between the ear closest to (ipsilateral) and the ear farthest from (contralateral) the sound source [5]. If this fly had the same directional hearing that most mammals have, then it would be impossible to determine the direction of sound given the differences described above. However, the *Ormia ochracea* has the ability to determine the direction of the chirping cricket. How does this fly accomplish this seemingly difficult task?

First, we need to understand the fly's auditory anatomy. A complex array of physiological mechanisms converts acoustic energy in the sound field into mechanical vibrations then sensed by the auditory sensory organs [1]. Figure 1

shows that the fly's ears are located in front and between the coxae of the prothoracic legs, below the neck and behind the head [2].

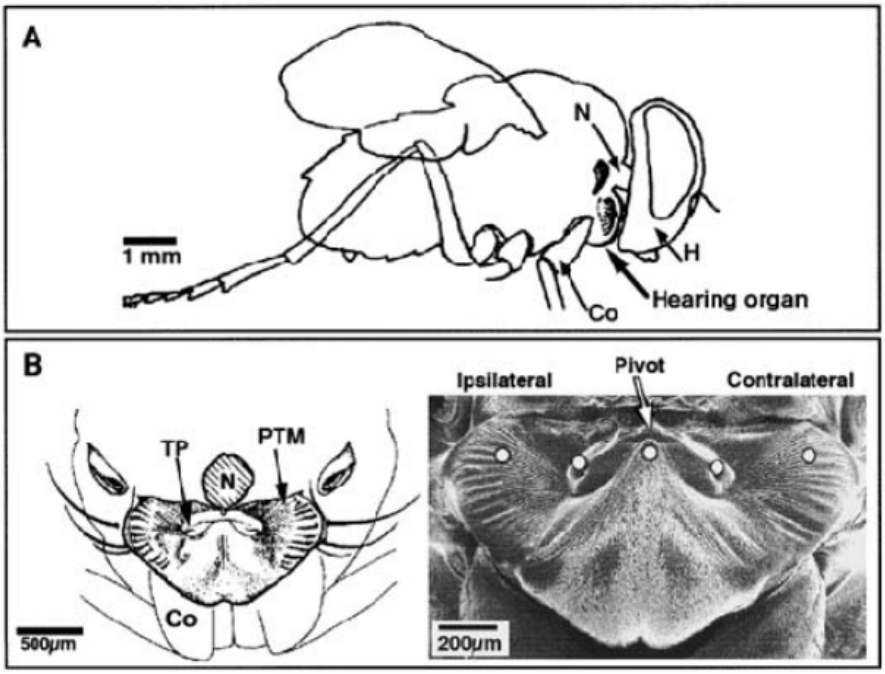

Figure 1. External anatomy of the ears of *Ormia Ochracea* (From: Miles et al., 1995).

The fly has two thin cuticular membranes prosternum (prosternal tympanal membranes – PTM) that are the main receivers for sound. These membranes connect to a pair of auditory sensory organs, the bulbae acusticae, which are located within a common, air-filled chamber. The bulbae acusticae attach to the membranes via a ridge-like in-growth of the exoskeleton (apodeme), which resembles a stiff rod. In effect, the PTM receives the signal and transfers the sound energy through the rod activating the bulbae acusticae. Each bulba acustica contains 70–75 auditory receptor cells, which transfer the signals to the nervous system of the fly [2]. For additional information, Robert et al [6] gives a complete and more detailed description of the anatomy.

The fly's auditory system has a mechanical connection between the two PTMs, called the intertympanal bridge. Figure 2 shows the mechanical model for

the hearing organ. As an incident sound wave hits the ipsilateral PTM, the coupling of the intertympanal bridge forces the contralateral PTM to move in the opposite direction. When a sound wave contacts an already displaced contralateral PTM, it forces the PTM in the opposite direction causing a bending motion about the intertympanal bridge. The PTM closest to the sound achieves greater amplitude than the PTM furthest from the sound. As a result, the neural sensory cells in the ear closest to the sound will fire with dramatically less latency than those of the opposite ear. This reduced latency provides the central nervous system with the essential information about the location of the sound source [7].

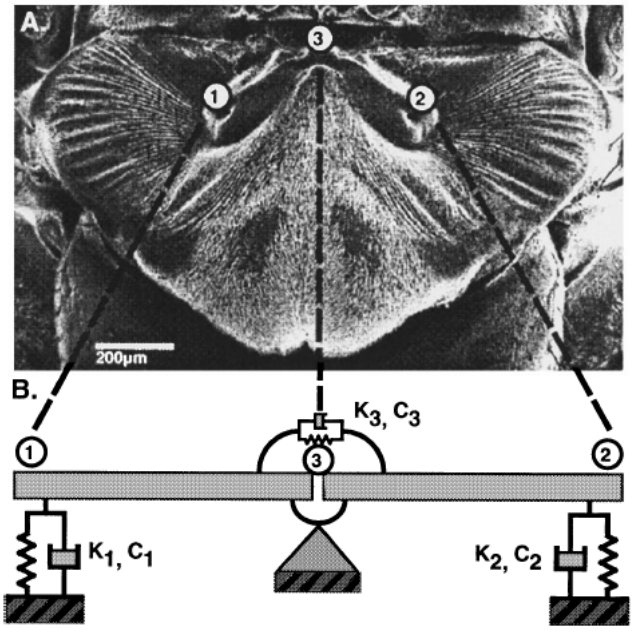

Figure 2. Mechanical model of the fly's ear (From: Miles et al., 1995).

II. SENSOR DESIGN

A. FABRICATED MEMS SENSOR CHIP

Previous generations of the devices at NPS used a 10 μm thick device layer. The bending mode eigen frequency of these devices was approximately 5 kHz. The design process for these 7th generation devices requires consideration of several factors. Increasing the rotational spring constant of the beam, without a significant increase in the inertia, leads to an increased bending mode eigen frequency. The next section describes the calculations of the spring constants and the eigen frequencies in detail. The previous generations used a bowtie sensor configuration with perforated wings and non-perforated wings as shown in Figure 3.

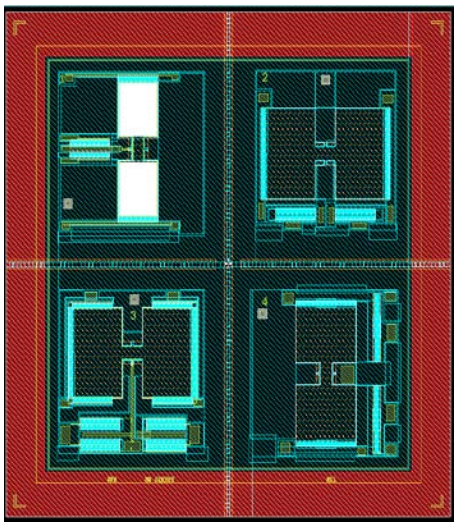

Figure 3. Generation 7 sensor design with 10 μm device layer.

The design process of these high frequency devices uses similar configurations and parameters to those used in previous generations. When calculating the rotational spring constant, the width of the bridge, the thickness of the device, and the length of the bridge are the only controllable parameters. The only controllable parameters for the moment of inertia calculation are the wing length and width, the bridge length and width, and the device layer

thickness. The eigen frequency is directly proportional to the device layer thickness. The high frequency devices have a $25\mu m$ device layer thickness. Three of the six high frequency devices use the bow-tie configuration used by the previous generations, while three of the devices use a new concept introduced in this generation. The new design only allows a bending mode of operation. The new design fixes the wings to the substrate and only permits the device to bend in the center. Figure 4 shows the fabricated high frequency MEMS sensors. Figure 5 shows the device dimension variables. Table 1 gives the dimensions of each device. Devices 1, 5, and 6 do not have a leg dimension since the wings are fixed to the substrate.

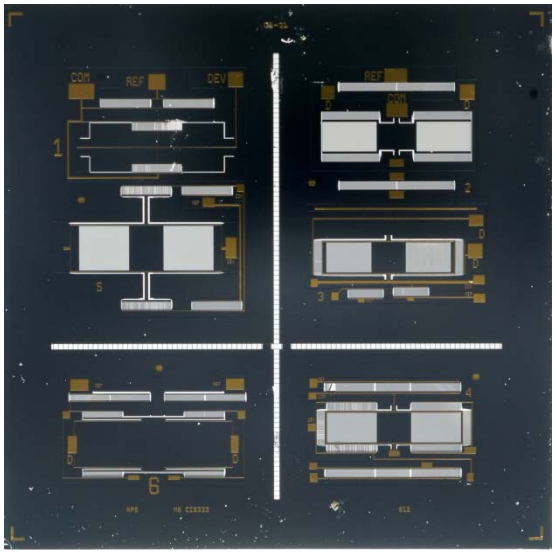

Figure 4. Photograph of generation 7 sensors with $25\mu m$ device layer.

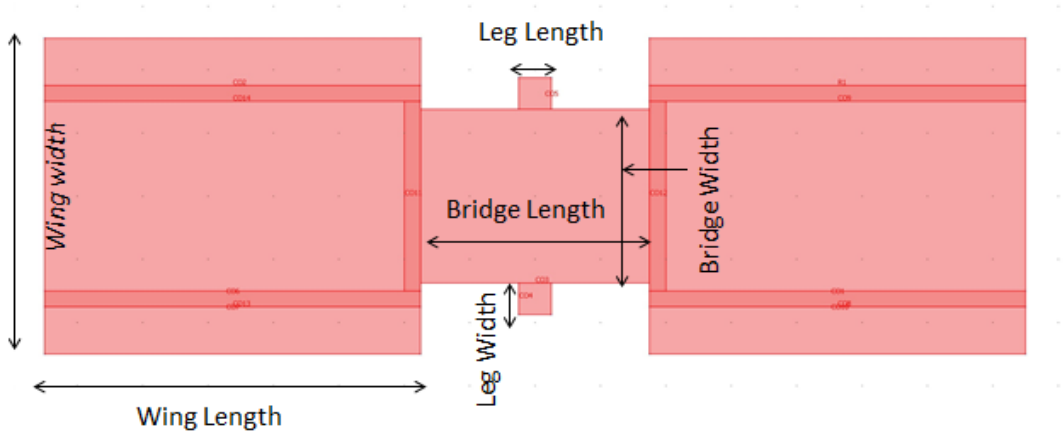

Figure 5. Sensor design dimensions.

Table 1. Generation 7 device dimensions.

Device	Wing width (μm)	Wing length (μm)	Bridge width (μm)	Bridge length (μm)	Leg width (μm)	Leg length (μm)
1	1000	850	700	1000	N/A	N/A
2	600	1150	550	700	100	100
3	700	900	700	700	100	100
4	700	1000	700	700	100	100
5	1000	1000	700	1000	N/A	N/A
6	1120	1175	1120	500	N/A	N/A

B. CALCULATION OF EIGEN FREQUENCIES

The eigen frequencies are calculated using the Lagrangian of the system using potential energies for the two modes and has the form [8, p. 13]:

$$L = T - V = \frac{1}{2} I \dot{\theta}_1^2 + \frac{1}{2} I \dot{\theta}_1^2 - K_p \left(\frac{\theta_1 + \theta_2}{2} \right)^2 - K_l \left(\frac{\theta_1 - \theta_2}{2} \right)^2 \tag{2.1}$$

where K_p is the rotational spring constant of the beam, K_l is the torsional spring constant of the bar, and I is the moment of inertia of the wing and half the bridge as they rotate about the y-axis.

The equation of motion is [8, p. 13]

$$\frac{d}{dt}\left(\frac{\partial L}{\partial \dot{\theta}}\right)=\frac{\partial L}{\partial \theta} \Rightarrow \frac{d}{dt}\left(I\dot{\theta}\right)=-K_p\left(\frac{\theta_1+\theta_2}{2}\right)-K_l\left(\frac{\theta_1-\theta_2}{2}\right)$$

Substituting θ_1 and θ_2, we get [8, p. 14]

$$I\ddot{\theta}_1=-K_p\left(\frac{\theta_1+\theta_2}{2}\right)-K_l\left(\frac{\theta_1-\theta_2}{2}\right) \text{ and} \tag{2.2}$$

$$I\ddot{\theta}_2=-K_p\left(\frac{\theta_1+\theta_2}{2}\right)+K_l\left(\frac{\theta_1-\theta_2}{2}\right) \tag{2.3}$$

Assuming harmonic dependence of angles, $\theta_1=\theta$ and $\theta_2=-\theta$ for the rocking motion, and $\theta_1=\theta_2=\theta$ for the bending motion, we can solve for ω in each equation with the following results [8, p.14]:

$$\omega_{rocking}=\sqrt{\frac{K_l}{I}} \tag{2.4}$$

$$\omega_{bending}=\sqrt{\frac{K_p}{I}} \tag{2.5}$$

The moment of inertia of the wing and half of the bridge as they rotate around the y-axis is [8, p.8]

$$I_{yy}=\rho\left(\int_0^h x^2dx\int_{-w/2}^{w/2}dy\int_{-t/2}^{t/2}dz\right)+\rho\left(\int_{l_1}^{l_1+l_2}x^2dx\int_{-l_3/2}^{l_3/2}dy\int_{-t/2}^{t/2}dz\right) \tag{2.6}$$

$$=\rho\left(\left[\frac{x^3}{3}\right]_0^{l_2}wt+\left[\frac{x^3}{3}\right]_{l_1}^{l_1+l_2}l_3t\right)=\rho\left(\frac{{l_1}^3}{3}wt+\frac{\left(l_1+l_2\right)^3-{l_1}^3}{3}l_3t\right) \tag{2.7}$$

$$= \frac{\rho t}{3}\left[l_1^3 w + \left(\left(l_1 + l_2 \right)^3 - l_1^3 \right) l_3 \right]$$

where $l_1 = \frac{1}{2}$ bridge length, $l_2 =$ length of wing, $l_3 =$ width of wing, $t =$ thickness of device layer, and $w =$ width of bridge.

The torsional moment of inertia *J* of a rectangular bar with width (w) and thickness (t) is: [8, p.11]

$$J = \left(\frac{w}{2} \right) \left(\frac{t}{2} \right)^3 \left[\frac{16}{3} - 3.36 \frac{t}{w} \left(1 - \frac{t^4}{12 w^4} \right) \right] \tag{2.8}$$

The torsional spring constant of the bar (K_l) and the rotational spring constant of the beam (K_p) are as follows: [8, p.10, 12]

$$K_l = \frac{GJ}{l} \tag{2.9}$$

$$K_p = \frac{Ewt^3}{12 l_1} \tag{2.10}$$

where G = Shear Modulus, E = Young's Modulus, l = length of the bar, and $l_1 = \frac{1}{2}$ bridge length.

The values calculated using this approach are approximate due to the assumptions made in Ref. [8]. The values for each of the six devices were in the high frequency range. The use of COMSOL finite element modeling program produced values that were more accurate as shown in the following chapter.

THIS PAGE INTENTIONALLY LEFT BLANK

III. EXPERIMENTAL DATA ANALYSIS

A. EXPERIMENTAL SET UP

Figure 6 illustrates the laboratory setup used to measure the amplitudes of the devices when excited with sound. The experiment setup consists of a reference microphone, speaker on a rotating boom, laser vibrometer, and the devices themselves. Incident sound pressure is measure by placing a Brüel & Kjaer® model 4138, $\frac{1}{8}$" microphone directly over the sensor. It has a 0.939 mV/Pa sensitivity and a frequency response that is almost flat from 50 Hz to 20 kHz [9].

The sound source is a Selenium loudspeaker type DH200E attached to the internal signal generator in the VibSoft® software. VibSoft® allows the generation of pure tones. It also allows a periodic chirp over a range of various frequencies. Manually rotating the speaker boom adjusts the angle of sound incident on the device. The laser vibrometer was a Polytec® single point vibrometer model OFV 302, with a model OFV 2600 controller. The laser's purpose was to measure the displacement of the wings of the sensor with a precision on the order of tens of picometers [9].

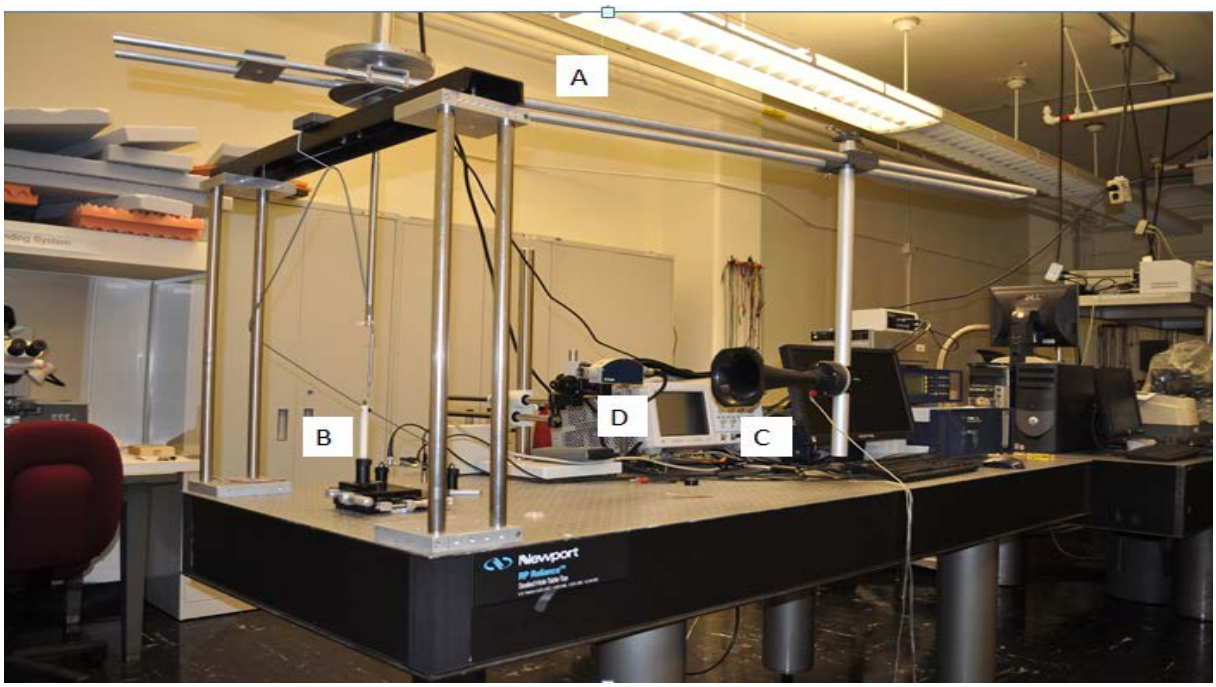

Figure 6. Lab equipment used for device testing. A. Rotating Boom. B. Device and reference microphone C. Speaker with directional horn. D. Laser vibrometer.

The sound source is attached to a rotating boom shown in Figure 7 and is used to measure the response of the devices at specific angles.

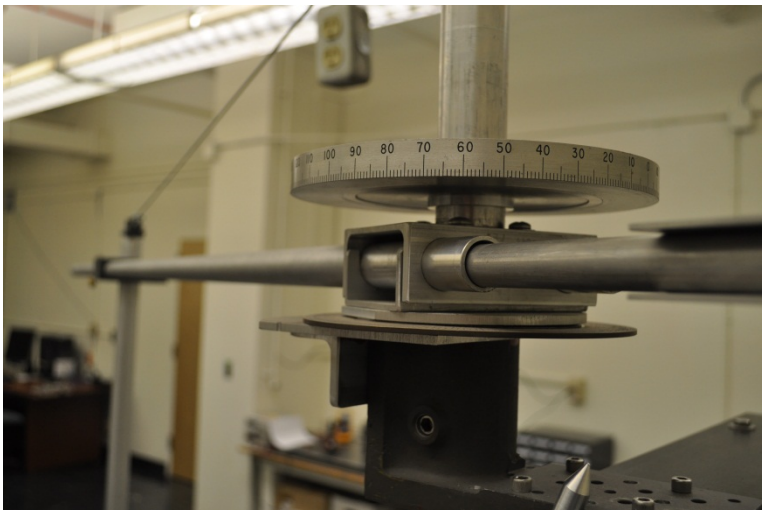

Figure 7. Rotating boom used for determining incident angle of sound.

The location of the reference microphone relative to the sensor chips is shown in Figure 8. The microphone connects to the reference input of the laser vibrometer [1].

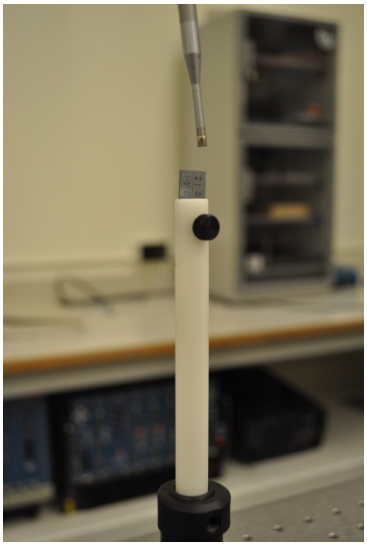

Figure 8. Sensor chip and reference microphone.

The sound source is the speaker shown in Figure 9. It has a horn to direct the sound toward the sensor.

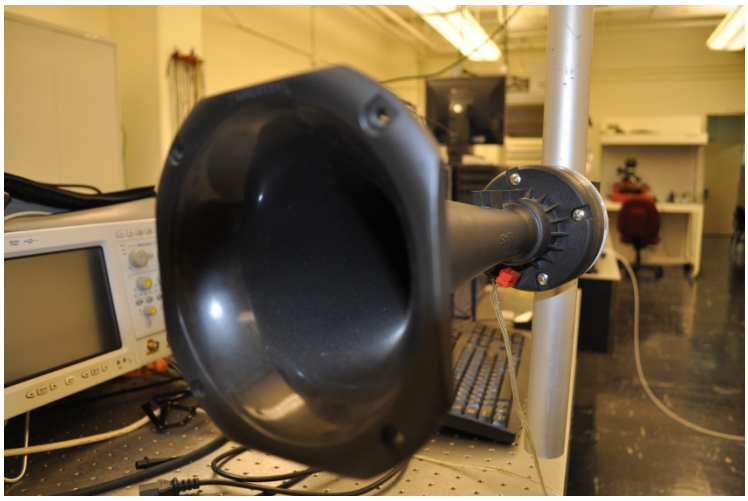

Figure 9. Sound source (speaker) with directional horn attached to it.

The laser vibrometer shown in Figure 10 measures the vibrational amplitudes of the wings in response to sound at different angles. Typically, the displacement is in the nanometer scale.

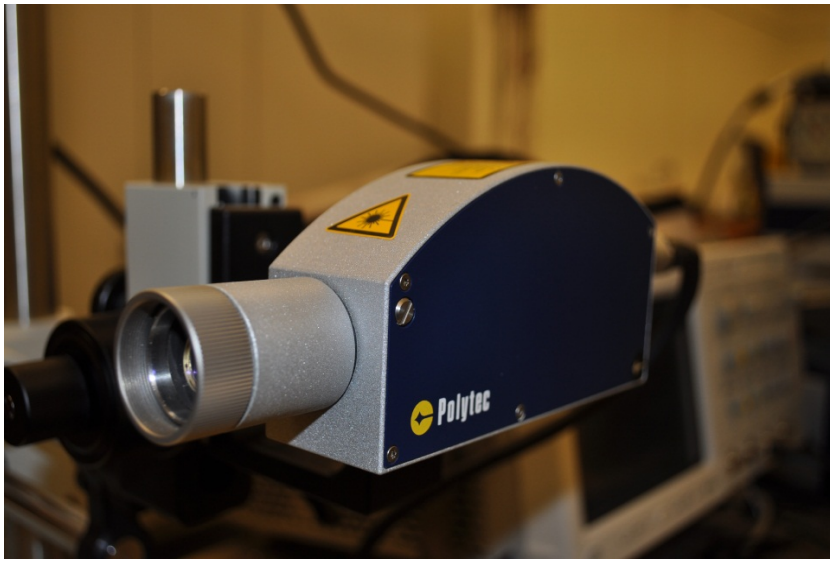

Figure 10. Polytec® laser vibrometer for measuring device displacement.

B. SIMULATED FREQUENCY RESPONSE (DEVICE 1–6)

A finite element analysis, using COMSOL, compares theoretical values to experimental values. Devices 1, 5, and 6 only have a bending mode associated with them due to the design. The edge of wings, fixed to the substrate, only allow movement in the center of the device as shown in Figure 11. These three devices also show different frequency and displacement amplitude response as shown in Figure 12. These three device responses are in good agreement with experimental data.

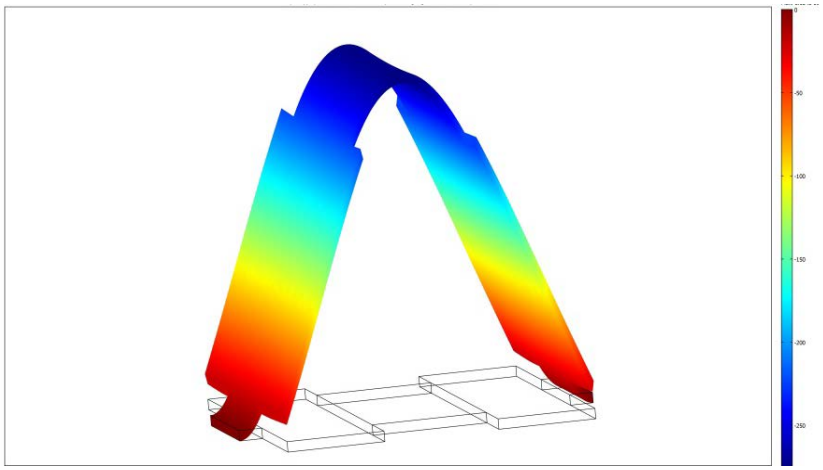

Figure 11. Bending mode deflection of device 1 under sound excitation.

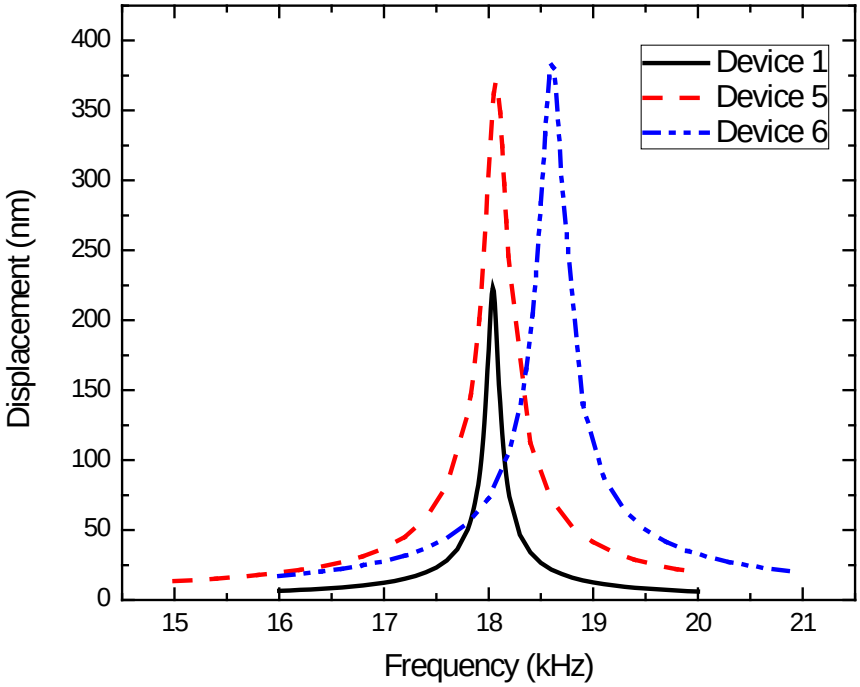

Figure 12. Simulated frequency response for Devices 1, 5, and 6.

Devices 2, 3, and 4 have a bending and rocking modes associated with them as in previous low frequency designs as shown in Figure 13. These three

devices also show different frequency and displacement amplitude response as shown in Figure 14. These three device responses are in good agreement with experimental data.

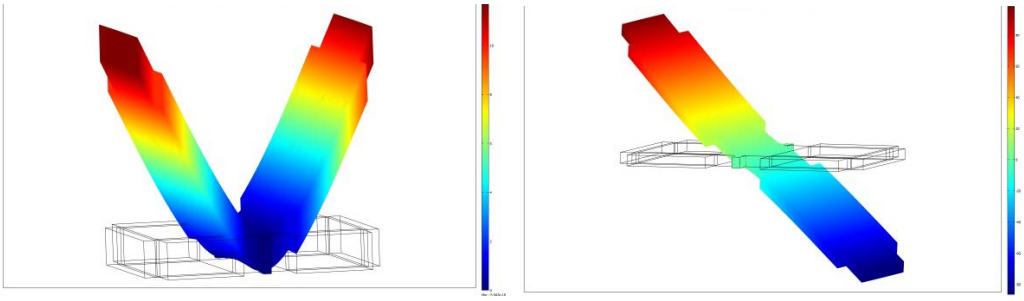

(a) (b)

Figure 13. Device 4 (a) bending and (b) rocking modes

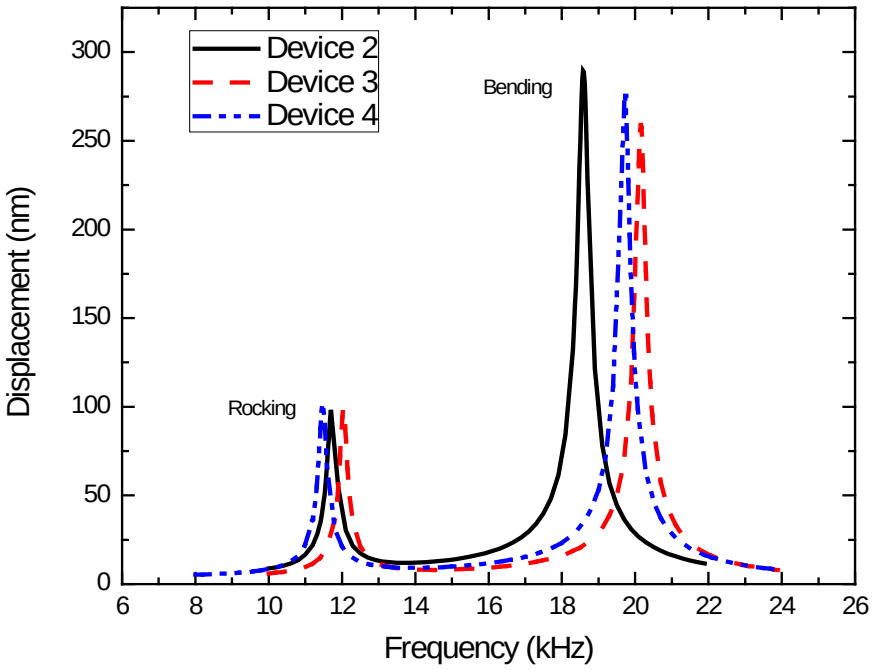

Figure 14. Simulated frequency response of Devices 2, 3, and 4 with rocking and bending mode responses.

C. MEASURED FREQUENCY RESPONSE (DEVICE 1–6)

The Polytec® laser vibrometer computed displacement amplitudes for the bending modes of all six devices. The rocking mode displacement amplitudes were very small due to the arrival time difference between the two wings and also fall outside the desired frequency range, therefore they were not measured in this thesis [8]. The bending mode amplitudes as a function of frequency are shown in Figure 14 and Figure 15. The angle of incident sound is 10°. The placement of the speaker and the laser vibrometer prohibited a perfect 0° angle of incidence for the sound source.

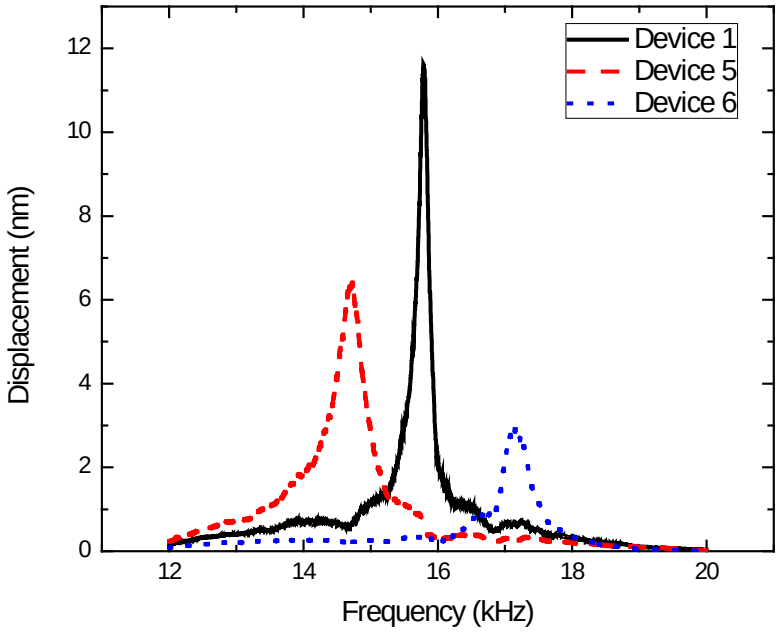

Figure 15. Measured bending mode frequencies of Devices 1, 5, and 6.

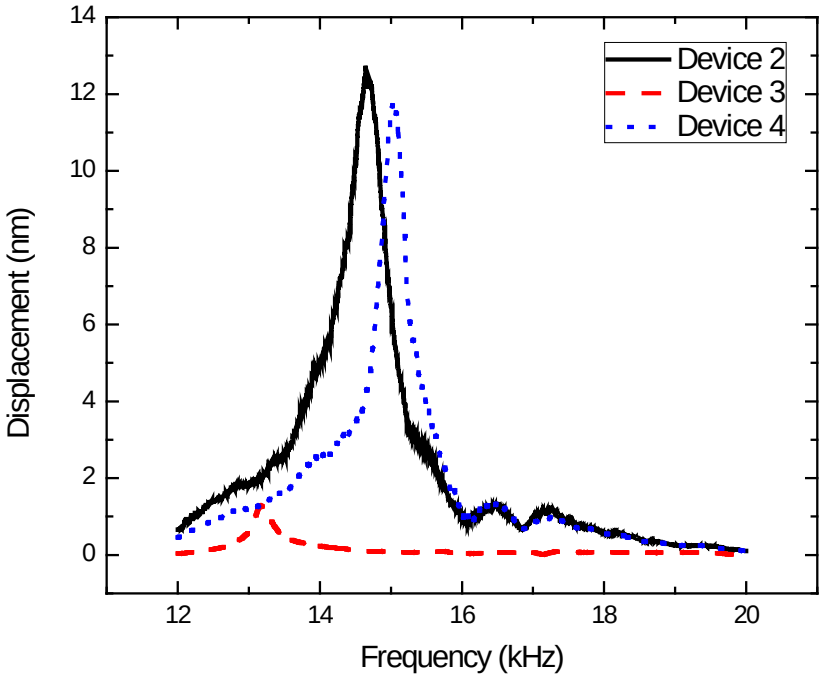

Figure 16. Measured bending mode frequencies of Devices 2, 3, and 4.

Applying 1 Volt to a controller connected to an amplifier for driving the speaker, sets the sound intensity. This generates an output voltage depending on the gain used to drive the sound source [9]. The reference microphone converts the signal to a pressure using the conversion factor of 0.939 mV/Pa, given by the manufacturer. Maximum bending amplitude displacement occurs on the wing's edge of devices 2, 3, and 4 and that is where the laser vibrometer is aligned. Maximum amplitude displacement of devices 1, 5, and 6 occur in the center of the devices and the laser vibrometer is aligned in the center for these devices. The measured bending mode frequencies are given in Table 2. All six devices show different frequencies as well as different amplitudes for the displacement.

Table 2. Simulated and measured bending mode frequencies with measured peak displacements of Devices 1–6.

Device	Simulated Bending Mode Frequency (kHz)	Measured Bending Mode Frequency (kHz)	Measured Peak Displacement (nm)
1	18.04	15.79	11.63
2	18.58	14.64	12.74
3	20.15	13.18	1.28
4	19.75	15.05	11.74
5	18.07	14.71	6.38
6	18.6	17.14	2.95

The simulated and measured frequencies all fall below the modeled device frequencies, usually about 3–4 kHz in most cases. The devices were modeled with a $25\,\mu m$ device layer thickness. The fabrication process is accurate to within $\pm 1\mu m$, which can affect the actual frequency response of the device. A device layer thickness of less than $25\,\mu m$ will lower the eigen frequency. During the experiment, we discovered the substrate oscillates with a harmonic frequency much like a cantilever. The frequency response of the substrate is dependent on how tight the substrate is fixed to the device holder, pictured in Figure 8. The tighter the substrate, the less the effect of this oscillation affects the eigen frequency of the device. Fixing the substrate on all four sides will also counter this effect. COMSOL simulation verified this effect with a shift in frequencies approximately 3 kHz.

D. BENDING MODE AMPLITUDE WITH INCIDENCE ANGLE OF SOUND

The goal of the device is to be able to determine direction of sound. In a pressure gradient microphone, the driving force is proportional to the pressure difference acting on the two sides of the diaphragm. The angle of incidence θ is

measured with respect to the normal to the diaphragm and the baffle as shown in Figure 17 [10]. When a sound wave hits the top surface of the sensor, it is diffracted and reaches the bottom side with a time delay corresponding to some effective travel path at normal incidence, L. The net sound pressure is a linear combination of the incident and diffracted components and is given by [4, p.2]

$$P = P_0\left(1 - e^{jkL\cos\theta}\right) \tag{3.1}$$

where k is the wavenumber and P_0 is the amplitude of incident sound. If the wavelength is much larger than the dimensions of the sensor, Equation 3.1 can be reduced, using the Taylor series expansion, to

$$P_0 \approx \left[1 - \left(1 - \frac{j2\pi L}{\lambda}\cos\theta\right)\right] = P_0\frac{j2\pi L}{\lambda}\cos\theta$$

which shows a cosine dependence on the incident angle of sound.

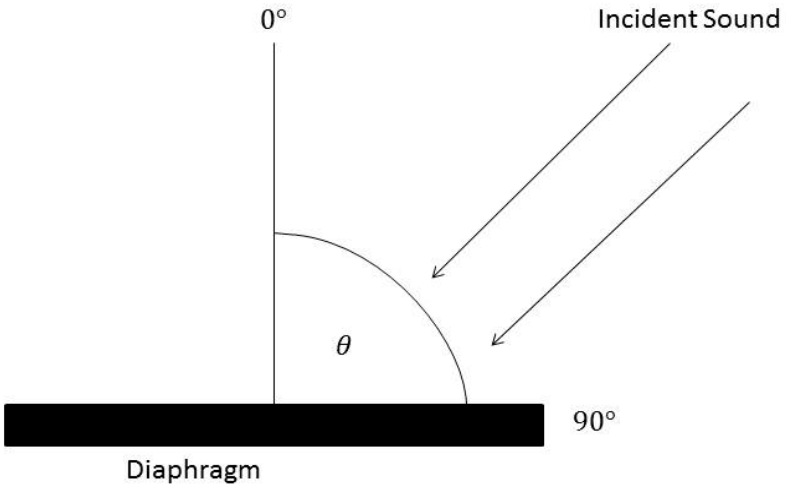

Figure 17. Directional response for a pressure gradient microphone.

The angle of incidence of sound varied from 10° to 90°. The behavior of all six devices, as expected, had cosine dependence. The intensity of sound was the same for all devices with an intensity of 0.939 V/Pa. Table 3 shows the values of the measured displacement and the value of the cosine.

Table 3. Measured displacement responses and cosine dependencies for different angles of sound incidence.

Angle (in Degrees)	**Device 1 Displacement (nm)**		**Device 2 Displacement (nm)**		**Device 2 Displacement (nm)**	
	Measured	**Cosine**	**Measured**	**Cosine**	**Measured**	**Cosine**
10	904.9	904.9	1027.5	1027.5	125.4	125.4
20	816.3	863.4	979.5	980.4	127.3	119.6
30	744.9	795.8	892.3	903.6	119.9	110.3
40	639.2	703.9	762.5	799.3	98.3	97.5
50	514.9	590.6	702.0	670.7	87.4	81.8
60	341.0	459.4	515.8	521.7	67.7	63.7
70	241.7	314.3	400.1	356.8	48.5	43.5
80	97.8	159.6	190.6	181.2	37.7	22.1
90	79.7	0	45.8	0	9.1	0
Angle (in Degrees)	Device 4 Displacement (nm)		Device 5 Displacement (nm)		Device 6 Displacement (nm)	
	Measured	Cosine	Measured	Cosine	Measured	Cosine
10	971.7	971.7	480.5	480.5	226.1	226.0
20	921.5	927.2	455.5	458.5	196.2	215.7
30	854.4	854.5	374.9	422.6	174.1	198.8

Angle (in Degrees)	Device 1 Displacement (nm)		Device 2 Displacement (nm)		Device 2 Displacement (nm)	
	Measured	**Cosine**	**Measured**	**Cosine**	**Measured**	**Cosine**
40	720.4	755.8	305.7	373.8	133.7	175.8
50	613.4	634.2	253.0	313.6	126.3	147.5
60	481.6	493.3	166.4	244.0	74.8	114.8
70	338.9	337.5	131.1	166.9	36.2	78.5
80	219.0	171.3	72.2	84.7	8.9	39.9
90	42.7	0	7.1	0	5.8	0.0

Figure 18 shows the response of device 4 and the cosine dependence as a function of angle of incident sound pressure.

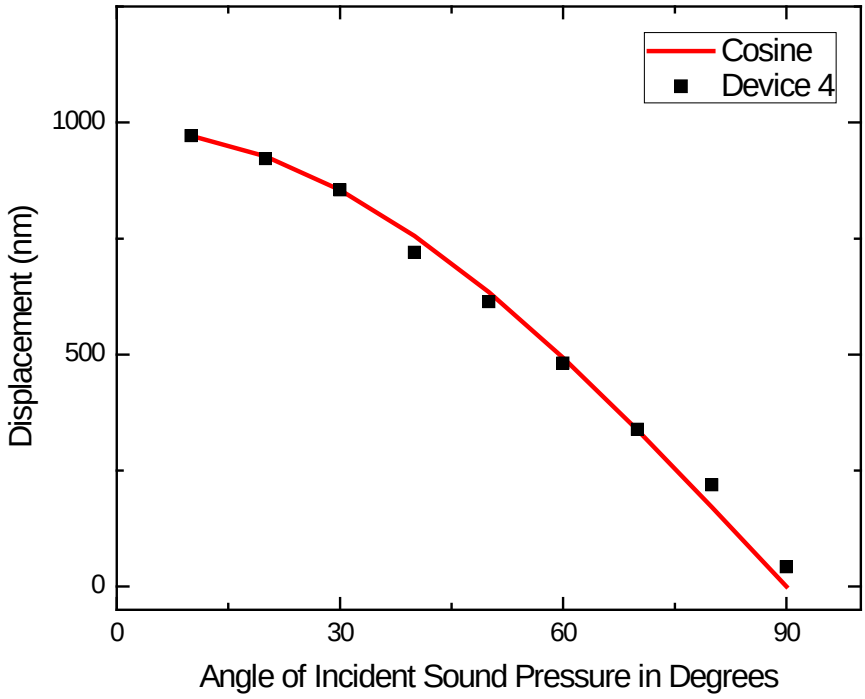

Figure 18. Measured displacement of device 4 and cosine dependence for different angles of sound incidence.

E. TRANSIENT TIME OF RESPONSE

The Polytec® laser vibrometer measured the transient responses of the six sensors at 10° angle of sound incident on each device. Each device responded as expected and Figures 19 and 20 shows the measured response. The second term in the equation of motion for a driven damped harmonic oscillator is the transient response, given by [11, p. 184]

$$x(t) = A\cos(\omega t - \delta) + A_{tr} e^{-\frac{bt}{2m}} \cos(\omega_1 t - \delta_{tr}) \tag{3.2}$$

From Equation 3.3, the time constant (τ) is derived and is $\frac{2m}{b}$, where b is the damping coefficient and m is the mass. Using the formula given by [12], the damping coefficient per unit area is given by

$$C_{damping} = \pi\sqrt{2\rho\omega\mu} \tag{3.3}$$

where ρ is the density of air and μ is the viscosity of air. When using the moment of inertia to determine the time constant (τ) use (*I)* in place of (*m)*. In addition, it is important to note, the final damping must be multiplied by area since *I* has units of $kg \cdot m^2$. Table 1 gives device dimensions for determining the area of each device.

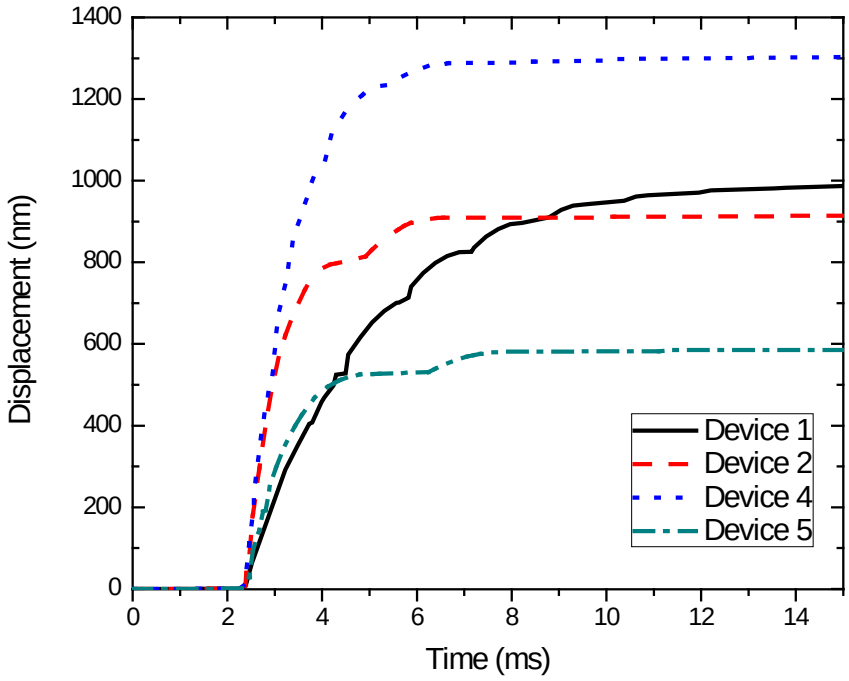

Figure 19. Measured transient times for Devices 1, 2, 4, and 5.

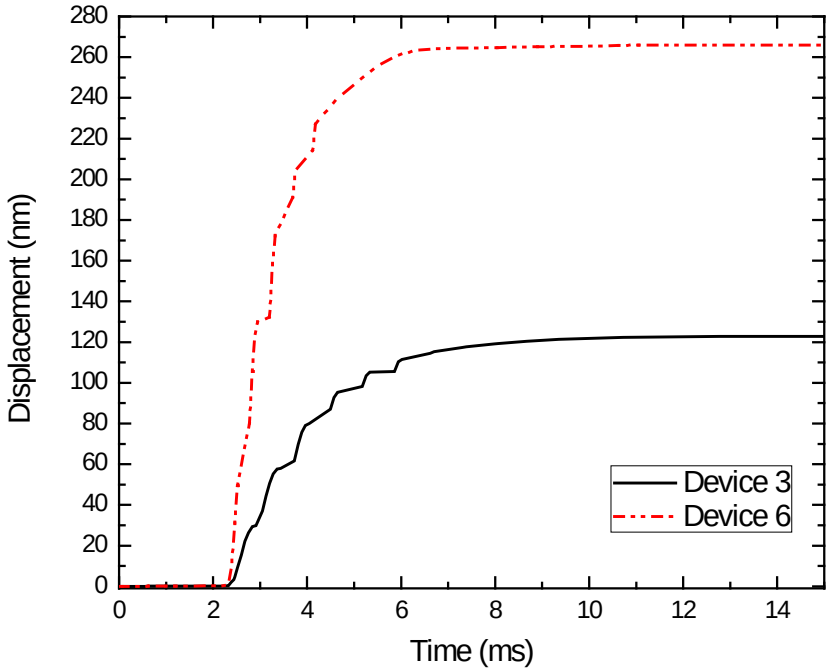

Figure 20. Measured transient times for Devices 3 and 6.

Devices 1 and 6 do not have perforated wings, which increases the mass of the device compared to the other devices. This increase in mass causes an increase in settling time. Devices 2, 4, and 5 have similar rise times due to the perforation of the wings. Device 3 has a smaller area as compared to the other devices, which increases its time. Table 4 gives approximated values for the measured transient times of all six devices.

Table 4. Transient times of Devices 1–6.

Device Number	Transient Time (ms)
1	8.6
2	5.8
3	6.0
4	5.7
5	4.1
6	6.1

F. EFFECTS OF PACKAGING AND SUBSTRATE

Device 4, shown in Figure 21, had the best directional response. Separating device 4 from the other devices allowed us to understand the device's response as an individual unit. The individual device underwent the same experimentation as described above. The device did not perform as expected. The device had little to no displacement response when tested over a range of frequencies. During the process of trying to understand the lack of displacement response, we observed the substrate acting as a cantilever beam. Testing with the laser vibrometer revealed a resonant frequency response from the substrate.

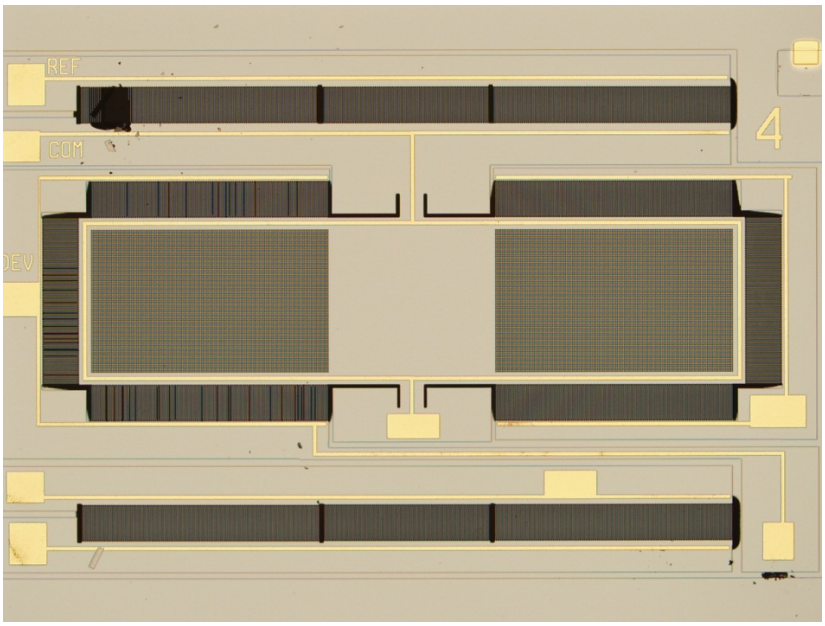

Figure 21. Photograph of Device 4

The frequency response of the device, once separated, had an amplitude response of about a few picometers. However, when individually testing generation 7 devices with a 10-μm device thickness that operates at low frequencies, it produced results that agreed with previous experiments. The resonant frequency of the previous devices was approximately 5 kHz and the wavelength of sound was about 7 cm. The resonant frequencies of the high frequency devices range from 13–18 kHz and wavelengths range from 1.9 to 2.6 cm. This is important to keep in mind when considering sound diffraction and interference.

The conclusion drawn from this experiment is that sound is diffracting around the sensor leading to a zero net pressure difference on the wings of the sensor. Equation 3.1 gives the net sound pressure. When Equation 3.1 is rewritten in the following form,

$$P = P_0 e^{\frac{-jkL\cos\theta}{2}} \left[e^{\frac{jkL\cos\theta}{2}} - e^{\frac{-jkL\cos\theta}{2}} \right] \tag{3.4}$$

Equation 3.4 simplifies to

$$P = P_0 e^{\frac{-jkL\cos\theta}{2}} \sin\left(\frac{kL}{2}\cos\theta\right) \tag{3.5}$$

Equation 3.5 shows that when $\sin\left(\frac{kL}{2}\cos\theta\right) = 0$ a zero net pressure difference is present on the two sides of the sensor. This leads to

$$\frac{kL}{2}\cos\theta = n\pi \tag{3.6}$$

Assuming normal incidence and solving for L, a zero net pressure occurs when $L = n\lambda$. When the path length difference is approximately an integer wavelength of sound, a zero net pressure will occur.

The device was mounted to a package, shown in Figure 22, and had a length about the size of the wavelength of sound. When the cavity of the package was covered, the device response drastically improved (see Figure 23) with a frequency closer to the simulated frequency, shown in Figure 14. This experiment verifies a zero net pressure on the wings occurs when $L \approx n\lambda$.

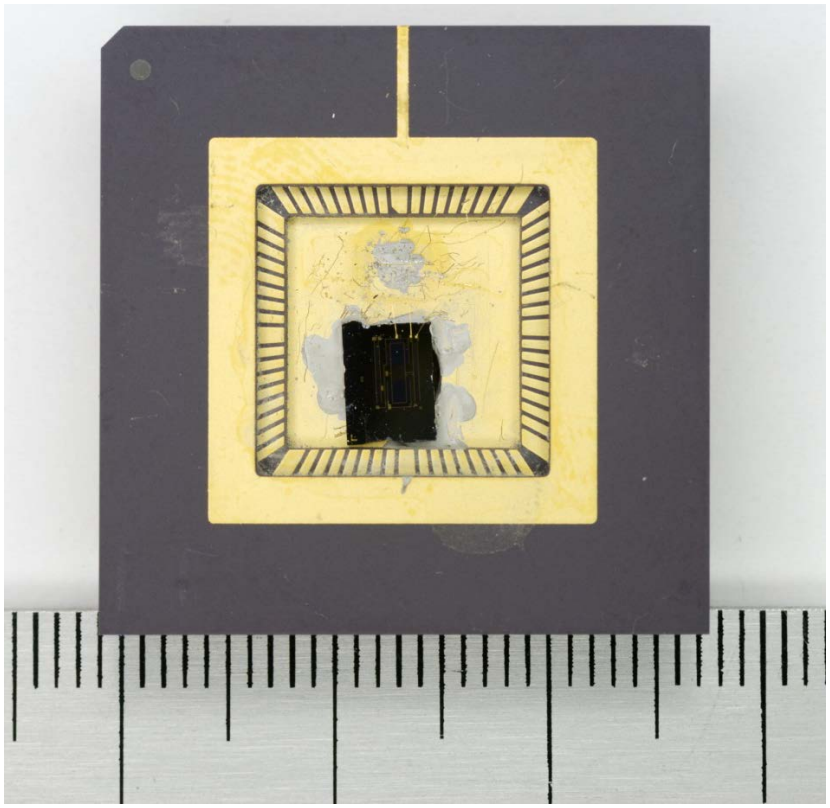

Figure 22. Photograph of Device 4 mounted to package with scale with increments of mm.

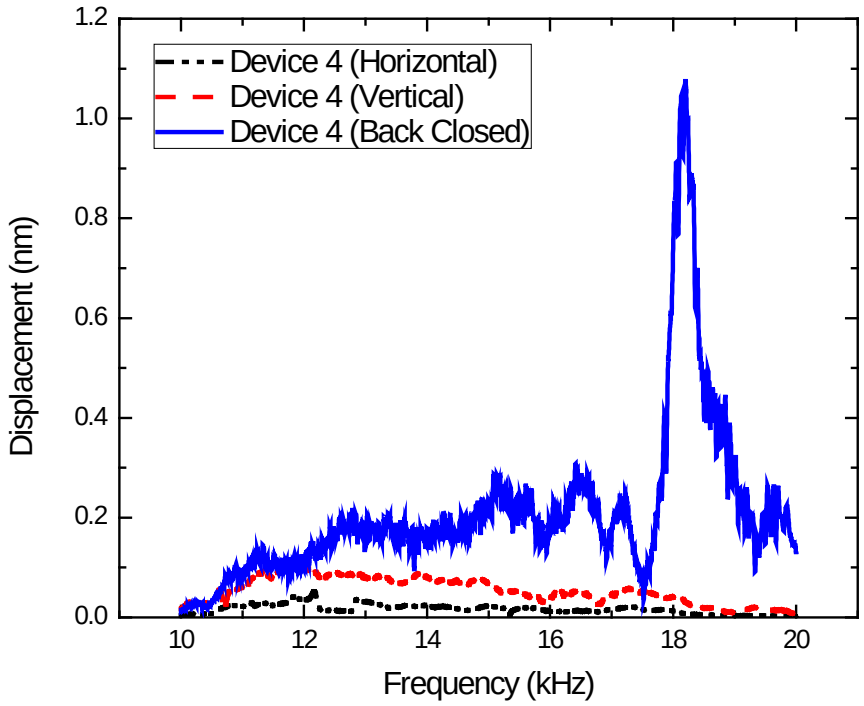

Figure 23. Measured frequency response of Device 4 with back of cavity closed compared to open cavity in the horizontal and vertical positions.

IV. CONCLUSIONS AND RECOMMENDATIONS

A. CONCLUSIONS

The structure of the auditory system of the fly *Ormia Ochracea* allowed for the characterization of a high frequency directional microphone. The initial performance was modeled and analyzed using COMSOL Multiphysics software. The main goal of this thesis was to characterize six high frequency sensors. Both designs show good directional response to sound, but the bow-tie design allows greater displacement amplitude, which will yield a higher electrical signal for future signal processing. It was also found that sound diffraction interference is present at the high frequency wavelengths and device packaging needs to be large enough to isolate the destructive interference. The measured and simulated response of the sensors showed relatively good agreement.

B. RECOMMENDATIONS

In order to achieve optimized performance of the high frequency sensors, it is recommended that future research be focused on designing and testing a sensor whose dimensions and packaging are small enough to eliminate a zero net pressure on the sensor. High frequency wavelengths are shorter compared to the previous generation devices. The dimensions of both the device, including the surrounding substrate, and the packaging are more important in order to maintain a pressure difference on the sensor. In addition, an electronic readout of the high frequency device is important to understand the strength of the electronic signal for varying angles of incidence of sound.

THIS PAGE INTENTIONALLY LEFT BLANK

LIST OF REFERENCES

[1] S. Harrison, “Free field modeling of a MEMS-based pressure gradient microphone,” M.S. thesis, Naval Postgraduate School, Monterey, California, January 2009.

[2] R.N. Miles, D. Robert, and R.R. Hoy, “Mechanically coupled ears for directional hearing in the parasitoid fly *Ormia Ochracea*.” *The Journal of the Acoustical Society of America* vol. 98, pp.3059–3070, December 1995.

[3] W. Cade, “Acoustically orienting parasitoids: fly phontaxis to cricket song,” *Science*, vol. 190, pp.1313–1313, 1975.

[4] M. Touse, J. Sinibaldi, K. Simsek, J. Catterlin, S. Harrison, and G. Karunasiri, “Fabrication of a microelectromechanical directional sound sensor with electronic readout using comb fingers,”*Applied Physics Letters,* vol. 96, pp. 1–3, April 2010.

[5] M. Akcakaya and A. Nehorai, “Performance analysis of the *Ormia ochracea’s* coupled ears,” vol. 124, pp. 2100–2105, October 2008.

[6] D. Robert, R.N. Miles, and R.R. Hoy, “Tympanal mechanics in the parasitoid fly *Ormia Ochracea.*” *Comp. Physiol A*., vol 183, pp.443–452, June 1998.

[7] R.N. Miles, Q. Su, W. Cui, M. Shetye, F.L. Degertekin, B. Bicen, C. Garcia, S. Jones, and N. Hall, “A low-noise differential microphone inspired by the ears of the parasitoid fly *Ormia ochracea.*” *The Journal of the Acoustical Society of America*, vol. 125, pp. 2013–2016, April 2009.

[8] D. Grevenitis. “Effects of substrate on response of MEMS directional sound sensor,” M.S. thesis, Naval Postgraduate School, Monterey, California, December 2010.

[9] N. Muamad, “Characterization of a MEMS directional microphone with solid and perforated wings,” M.S. thesis, Naval Postgraduate School, Monterey, California, January 2009.

[10] L.E. Kinsler, A.R. Frey, A.B. Coppens, and J.V. Sanders, *Fundamentals of Acoustics.* New York: Wiley and Sons, 2000.

[11] J. R. Taylor, *Classical Mechanics.* Sausalito: University Science Books, 2005.

[12] W. Zhang and K. Turner, “Frequency dependent fluid damping of micro/nano flexural resonators: Experiment, model and analysis,” *Sensors and Actuators A: Physical*, vol. 134, pp.594–599, 2007.

THIS PAGE INTENTIONALLY LEFT BLANK

INITIAL DISTRIBUTION LIST

1. Defense Technical Information Center
   Ft. Belvoir, Virginia

2. Dudley Knox Library
   Naval Postgraduate School
   Monterey, California

3. Andres Larraza
   Naval Postgraduate School
   Monterey, California

4. Gamani Karunasiri
   Naval Postgraduate School
   Monterey California

5. Bruce Denardo
   Naval Postgraduate School
   Monterey, California

6. Darren D. Davis
   Naval Postgraduate School
   Monterey, California

7. Captain David Price
   Naval Postgraduate School
   Monterey, California